metals

MDPI

Article

Growth and Coalescence of γ′-Precipitates in Nickel-Based Alloy 115NC during Slow Cooling for Membrane Manufacturing

Christian Voelter * and Joachim Rösler

Institut für Werkstoffe, Technische Universität Braunschweig, Langer Kamp 8, 38106 Braunschweig, Germany; j.roesler@tu-braunschweig.de

* Correspondence: c.voelter@tu-braunschweig.de

Abstract: By coarsening of the γ′-precipitates and selective extraction of one of the two existing phases, porous structures can be produced from nickel-based superalloys. There are two basic approaches to achieve a bicontinuous γ/γ′-microstructure—directional and incoherent coarsening. Single crystalline superalloy membranes are produced by the so-called rafting of the microstructure, i.e., directional coarsening. Unlike this process, incoherently coarsened membranes lack a detailed understanding of the mechanisms leading to cross-linking of the precipitates. In this paper, the growth and coalescence of precipitates during initial slow cooling from above the γ′ solvus temperature was studied. In addition to the three-dimensional morphological changes of the precipitates, it is also shown that only little coalescence of the particles occurs despite the high γ′ content and, therefore, their very small distance. The loss of coherency that occurs during this part of coarsening must first advance through further aging before a bicontinuous microstructure is formed.

Keywords: γ′ precipitates; morphology evolution; growth of γ′; coalescence; superalloy membranes

check for updates

Citation: Voelter, C.; Rösler, J. Growth and Coalescence of γ′-Precipitates in Nickel-Based Alloy 115NC during Slow Cooling for Membrane Manufacturing. *Metals* **2022**, *12*, 134. https://doi.org/10.3390/met12010134

Academic Editor: Yoshihiro Terada

Received: 3 November 2021
Accepted: 5 January 2022
Published: 11 January 2022

Publisher's Note: MDPI stays neutral with regard to jurisdictional claims in published maps and institutional affiliations.

Copyright: © 2022 by the authors. Licensee MDPI, Basel, Switzerland. This article is an open access article distributed under the terms and conditions of the Creative Commons Attribution (CC BY) license (https://creativecommons.org/licenses/by/4.0/).

1. Introduction

Nickel-based superalloys are well known for their applications at high temperatures and loads. After solution and precipitation heat treatment, the initial microstructure consists typically of regularly arranged cubic γ′-particles coherently embedded in the γ-matrix. However, external stresses at high temperatures cause the particles to coarsen directionally [1–4]. This phenomenon, also called rafting, can be used to produce nanoporous superalloy membranes [5–8]. The coarsening leads to coalescence of the precipitates and finally to a bicontinuous γ/γ′-microstructure. This microstructure can be obtained both by creep deformation [5–8] and by rolling at room temperature followed by aging [8]. The first method is typically used for single crystalline alloys, while the second is also suitable for polycrystalline alloys. In both cases, an open porous structure is formed subsequently by (electro-)chemical extraction of either the γ- or γ′-phase. In single crystals it is even possible to use internal stresses, the so-called dendritic stresses [9], to form a bicontinuous γ/γ′-microstructure and, thus, nanoporous superalloy membranes [10]. All these methods have the same principal procedure in common: first, a microstructure consisting of cubic γ′-precipitates coherently embedded in the γ-matrix is produced by classical solution and precipitation heat treatment. Second, triggered by creep deformation, plastic deformation or internal stresses, directional coarsening of the γ′-precipitates is utilized to obtain a bicontinuous γ/γ′-microstructure. Third, one phase is extracted to produce the final membrane.

Initially, it was our belief that directional coarsening of the coherent γ′-phase is indispensable to obtain a bicontinuous γ/γ′-microstructure and, thus, a superalloy membrane after selective phase extraction. However, [11,12] show that this is not necessarily so. In those studies, the single crystalline superalloy CMSX-4 was used to fabricate membranes depending on the cooling rate from the solutioning temperature. Air cooling and a cooling rate

of 4 K/min, followed by extended exposure at 1080 °C, led to the typical formation of a bicontinuous γ/γ'-microstructure due to rafting of coherent γ'-particles. However, at cooling rates of 1 K/min and 0.2 K/min, large irregularly shaped γ'-particles formed, which apparently lost coherency and, consequently, showed no sign of rafting. Nevertheless, it was possible to produce membranes. Similar results were obtained on the polycrystalline superalloy 115NC [13–15], which is a carbon-free version of Nimonic 115 [16]. In [15], the material was simply heat treated above the γ' solvus temperature (1200 °C/10 min), slowly cooled at 1 K/min to 1100 °C followed by a final air cooling (AC), and then heat treated for an extended period of time in the γ/γ' two phase field (1020 °C/4 h/AC + 1000 °C/144 h/AC). Again, membrane fabrication was possible even though large, apparently incoherent γ'-particles formed and rafting, which requires coherency between γ'-particles and γ-matrix, did not take place. Despite the simplicity of the procedure, the final polycrystalline membranes exhibited a tensile strength of more than 100 MPa [15], exceeding that of single crystalline membranes fabricated by directional coarsening through creep deformation [7].

Given these results, fabrication of membranes from the polycrystalline superalloy 115NC via slow cooling is apparently quite attractive. Obviously, a bicontinuous γ/γ'-microstructure must have formed during the aforementioned heat treatment, despite the absence of directional coarsening. Otherwise, membrane fabrication by selective phase extraction would not have been possible. Two-dimensional micrographs, taken after the entire heat treatment procedure was completed, showed γ'-particles in the form of octodendrites connecting at their tips [15]. It was assumed that this mechanism leads to the required bicontinuous microstructure. However, a detailed understanding is still missing. Currently, it is neither clear how the microstructure develops in the course of the heat treatment process nor is it possible to fully appreciate its three-dimensional nature from 2D sections. This is unfortunate because the microstructural evolution and the final properties of this novel membrane material are interdependent. Consequently, the objective of this paper is to close this gap. In this article, we concentrate on the microstructure evolution of the superalloy 115NC during slow cooling from solutioning with particular attention to the growth and cross-linking (i.e., coalescence) of neighboring γ'-particles. For this purpose, interrupted heat treatment experiments were conducted. In addition to micrographs, particle extraction and deep etching were used to gain further insights.

2. Materials and Methods

In this article, we examined the superalloy 115NC, which is the carbon-free version of Nimonic 115. Its exact composition is Ni-14.4Cr-13.2Co-5Al-3.8Ti-3.3Mo-0.05Zr-0.02B-0.044Mg (in wt.%). The material was cast by plasma arc melting into plates measuring 60 × 60 × 3 mm and then separated into individual samples of approximately 10 × 10 × 3 mm. To investigate the slow cooling from above γ'-solvus and, thereby, the increasing volume fraction as well as the coarsening of the γ'-phase, 14 samples were examined. All samples were first solution heat treated at 1200 °C for 10 min and then slowly cooled in the furnace at 1 K/min. To study the process of precipitation growth, samples were taken from the furnace at different temperatures and water quenched. The first sample was taken at 1185 °C, the last at 900 °C. According to calculations in Thermo-Calc, 1185 °C corresponds to the γ' solvus temperature, while 1140 °C–1160 °C is given in [17] for Nimonic 115. With the exception of the first temperatures, each sample was taken after further cooling by 25 K. Since the opening of the furnace door might have an influence on the other samples in the furnace, the heat treatments performed together in one furnace run are documented in Table 1. At the beginning of the precipitation in particular, an influence of opening the furnace door should be eliminated, so that the first samples were heat treated separately.

Table 1. Overview of the heat treatments performed. Each sample is first solution heat treated at 1200 °C for 10 min and then cooled to the specified temperature at 1 K/min. The furnace run number shows which samples were pooled together in one furnace run.

Furnace Run Number	Cooling to . . .
1	1185 °C
2	1175 °C
3	1165 °C
4	1150 °C 1125 °C 1100 °C
5	1075 °C 1050 °C 1025 °C 1000 °C 975 °C 950 °C 925 °C 900 °C

To examine the γ′-precipitates, the samples were prepared for different methods. First, micrographs were made in a scanning electron microscope (SEM; Zeiss LEO 1550), for which the samples were ground (grit P240 to P2500), polished (diamond suspension 9 µm to 1 µm and oxide polishing suspension 0.05 µm) and etched (molybdic acid etchant: 100 mL dist. H_2O, 100 mL HNO_3 (65%), 100 mL HCl (37%), 3 g MoO_3 powder for 4 s; attacks γ′-phase).

Since only a 2D image can be obtained in this way, but the 3D shape of the γ′-particles is of interest, particle extraction and deep etching were also performed. For this, except for the previously polished surface, a protective lacquer was first applied to all sides of the sample, which is intended to limit the subsequent etching on the uncoated surface. Then, each sample was individually electrochemically etched (8 g citric acid and 8 g ammonium sulfate in 800 mL dist. H_2O) for 2 h at a constant current of 0.2 A/cm^2 with respect to the free sample area. Hereby, the γ-phase was selectively dissolved. The sample was then cleaned in a container filled with methanol in an ultrasonic bath. During this process, the loose γ′-particles disperse from the surface into the methanol and can then be applied to a silicon wafer with a swab. Both the loose γ′-particles and the deeply etched specimen were examined in the SEM.

3. Results

In the following, the results of the interrupted cooling experiments are described. All samples were first solution annealed in the single-phase field and then cooled at 1 K/min. The temperatures given in the following correspond to those at which the samples were removed from the furnace and water quenched.

After cooling to 1185 °C as well as to 1175 °C, a bidisperse microstructure with fine cubic and very fine round γ′-precipitates is found. The cubic precipitates at 1185 °C have an edge length of about 50 nm and the round ones a diameter of about 20 nm. At 1175 °C, the dimensions are about 80 nm and 20 nm, respectively. As slow cooling into the γ/γ′ two-phase field leads to a low nucleation rate but fast growth, these fine particles must have formed during the removal of the samples from the furnace and the subsequent cooling. Consequently, γ′-precipitation did not take place during furnace cooling.

The cooling to 1165 °C, Figure 1a, principally results in four precipitate sizes. Firstly, as with the previous temperatures (1185 °C and 1175 °C), fine cubic as well as very fine round particles are obtained (Figure 1b). The cubic precipitates have a size of about 120 nm and show first signs of growing cube corners, thus forming concave cube surfaces. The very fine

precipitates are in the range of 10–20 nm. Furthermore, coarse octodendritic precipitates of 1–5 µm in size are formed (see also Figure 2). In the diffusion zone around these coarse precipitates, one sees fine precipitates with a size in between those of the previously described fine cubic and very fine round ones. Clearly, the octodendritic particles are a result of the furnace cooling, while the fine particles stem from quenching. The observed shapes of the γ′-particles are in agreement with the well-known evolution from spheres to cubes, octocubes and octodendrites as individual γ′-particles grow [18].

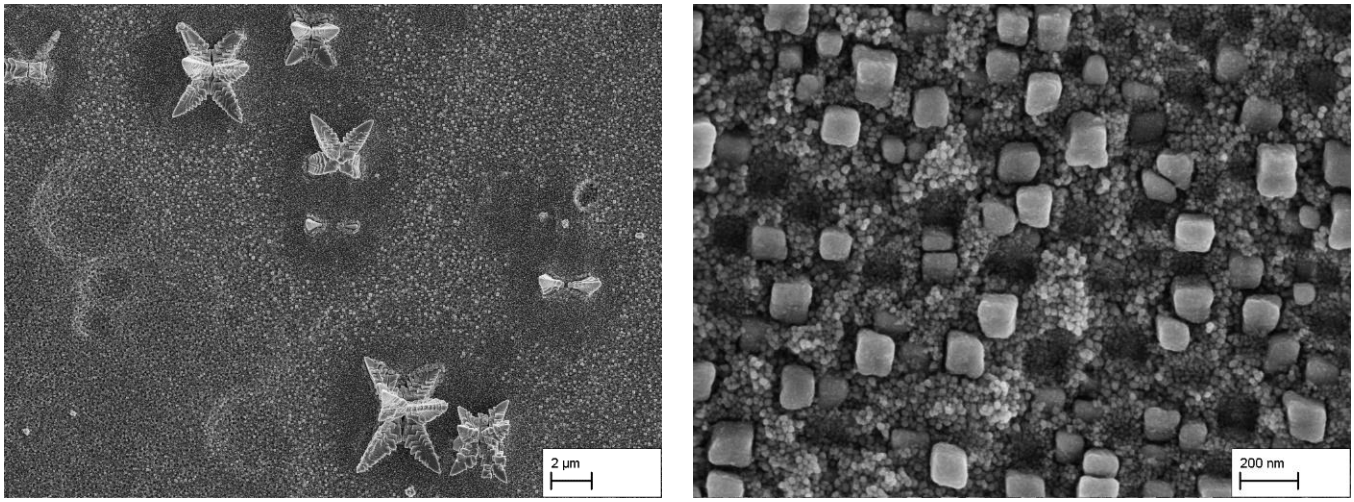

(**a**) (**b**)

Figure 1. Deeply etched specimen with γ′-precipitates after slow cooling to 1165 °C. (**a**) Coarse particles with visible diffusion zones around them and fine cubes along with very fine round particles due to rapid cooling in the surrounding areas. It can be seen that the diffusion zones of the individual coarse particles overlap only in a few cases. (**b**) Magnification of the precipitates due to the rapid cooling in the surrounding areas.

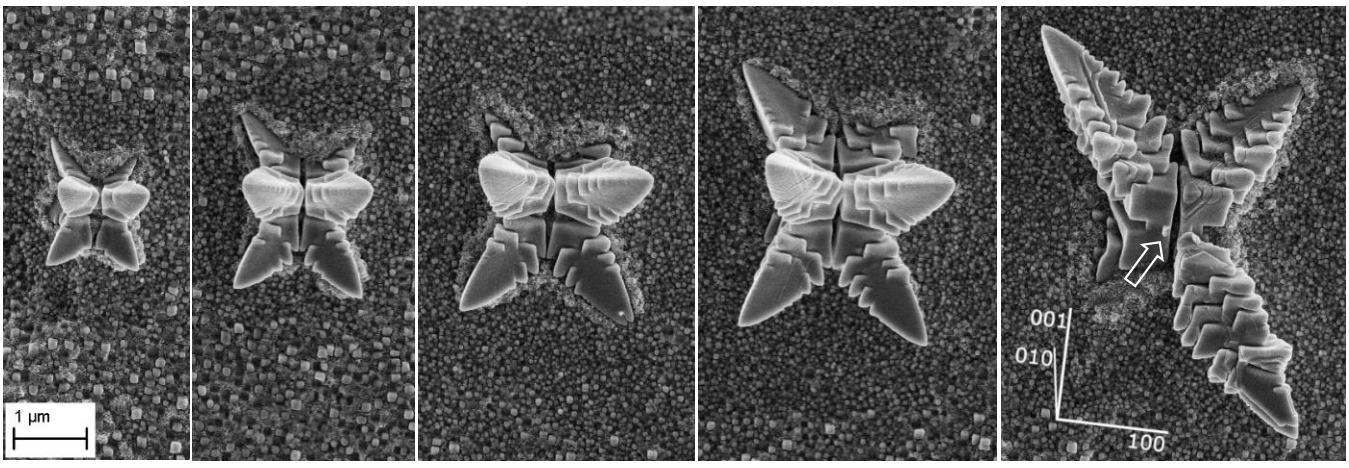

(**a**) (**b**) (**c**) (**d**) (**e**)

Figure 2. γ′-precipitates of different sizes after cooling to 1165 °C (deep etched specimen). Based on this sequence, the morphology change during the early stages of growth can be demonstrated. (**a**) Division in octocube already occurred, cube corners stretched in <111>-directions, first signs of steps at edges of stretched corners. (**b**) Particles grew as a whole (including the central octocube), number and size of steps at edges increased. (**c**,**d**) Further growth. (**e**) Significantly more pronounced steps, three of eight primary arms are no longer present. The arrow indicates a tiny contact area where the two missing arms seem to have been connected to the two remaining on the left side.

As shown in Figure 2, octodendrites of different sizes are observed in the sample cooled to 1165 °C. They must have formed at slightly different times and, consequently, grown to different sizes. Comparing these precipitates, the morphology change during growth can be followed very well. In its basic structure, each precipitate shows a complete or at least partially complete octocube with growth of the corners in <111>-directions, creating a star-like morphology. The cube corners grow faster because they protrude further into the supersaturated matrix, see e.g., [19,20]. With growth of these particles, both the central octocubes and the (dendrite) arms grow. Thereby a transformation of the morphology takes place and steps, parallel to the initial cube faces, i.e., parallel to {001}-planes, are formed at the three edges of the arms. After steps have formed, more {001}-oriented side faces evolve at these locations, resulting in shapes that might be best described as incomplete cubes (see, e.g., Figure 2e). Growth of the incomplete cubes starts at all three edges of a dendrite arm, meeting then in the middle of the faces of the dendrite arm with ongoing growth. The result demonstrates that at this stage of the cooling process, the dendrite arms remained at least partially coherent to the matrix. Otherwise, {001}-oriented side faces would not form.

In the center of the octodendrite one can clearly see the splitting of the central particle into octocubes. However, splitting is not always complete. Some channels are continuous and divide the cube in half, other matrix channels reach from the outside only partially to the center. Sometimes the channels are the widest in the center and taper outwards. Inspecting Figure 2d, at least the upper two dendrite arms are no longer embedded in the deeply etched matrix. Nevertheless, they did not fall off, demonstrating that these arms are connected at their base to the rest of the octodendrite. However, in Figure 2e, three of the eight arms did break or fall off. It seems that the two missing arms on the left had a tiny contact area to the other two arms on the left, which broke off (see arrow), while there is no visible contact area between the missing and remaining arm on the right. Another similar spot can be seen in Figure 3a, where the fracture area is in the center of the particle, of which one half broke off during specimen preparation.

In other precipitates, see e.g., the right particle in Figure 3b and the particles in a later cooling state in Figure 4, the incomplete cubes at the primary dendrite arms have continued to grow, now forming cube-like outgrowths, in the following also referred to as secondary branches. These secondary branches are also separated by narrow matrix channels, although it is not clear whether the γ-channels are present from the beginning or whether they are formed by further splitting. The outgrowths orient themselves with their surfaces to {100}-planes and form coherent interfaces. In the center of the precipitates, the smooth interfaces gradually disappear and more and more steps appear. Note also that the right particle in Figure 3b has more pronounced cube-like outgrowths than the left one despite its smaller size.

With further growth or further lowering of the temperature, precipitates with a diameter of up to 10 µm are formed. On the exterior of the particles in particular, cube-like outgrowths (edge length about 0.5–1 µm) can be seen (see white arrows in Figure 4), whose interfaces are the more coherent the smaller they are. The faces of these cubes align along {100}-planes. The two central precipitates in Figure 4a have these cubic outgrowths in the lower parts of the precipitate. The pyramid-like structure is formed because one (the upper) half of the octodendrite is not connected to the lower half and is removed during deep etching. This results in the inner areas of the precipitates becoming visible. The topmost area corresponds to the part where the original splitting took place, i.e., the center of the precipitate. In contrast to Figures 2 and 3, these areas show a high number of steps caused by interfacial dislocations (see inset in Figure 4a). At these areas the dislocation network is particularly pronounced, but in other areas they are also the rule. Only the exterior cubes show continuous smooth interfaces. In general, the coherency increases towards the exterior.

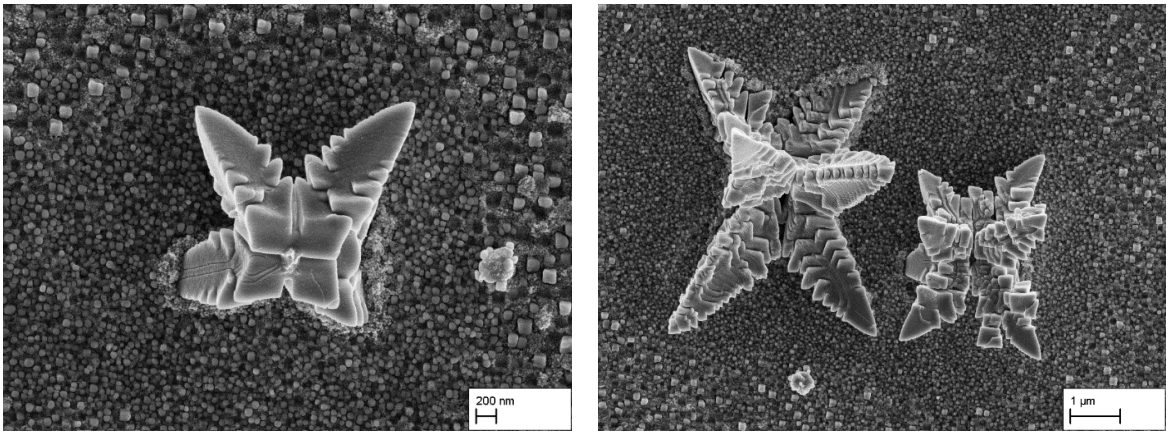

(**a**) (**b**)

Figure 3. Deeply etched specimen with γ′-precipitates after slow cooling to 1165 °C. (**a**) Half of a γ′-precipitate with a view of the central splitting channel. (**b**) Two separately grown precipitates nucleated near each other.

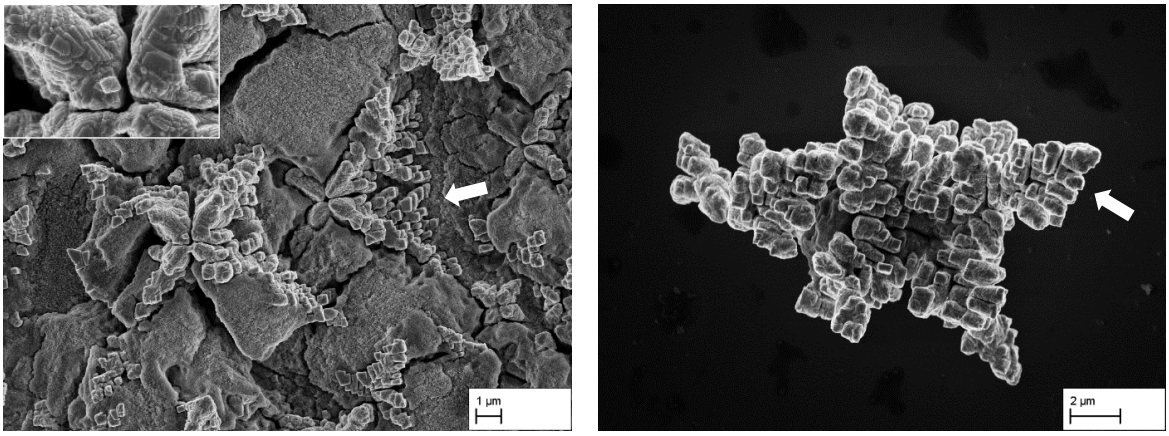

(**a**) (**b**)

Figure 4. (**a**) Half octodendrites in deeply etched specimen cooled to 1150 °C. Inner regions are covered with steps caused by interfacial dislocations and with little cubic characteristics. These steps can be seen in the three times magnified image detail. (**b**) Extracted particle from specimen cooled to 1100 °C with cube-like outgrowth at the outer regions. In both pictures, white arrows exemplarily indicate those outgrowths.

These smooth surfaces are only observed on outgrowths below 1 µm edge length. Furthermore, these small branches are also more separated from each other by γ-channels. Figure 5a shows both the cube-like outgrowths and the less coherent inner interfaces. Note, two of the eight dendrite arms did break or fall off here as illustrated in Figure 5b, so that the interfaces of the inner splitting channels are revealed. The larger the branches become, the more incoherent they become and more steps appear at the interfaces (see also Figure 6a).

As the growth proceeds, the pronounced star-shaped morphology is progressively lost and more compact blocks are formed (Figures 5a and 6). In other words, the prominence of the arms, i.e., the elongation in <111>-directions, decreases. The large number of small cubic outgrowths become coarser, more or less cuboidal blocks with less coherent faces.

A key issue in this study is the behavior of the precipitating particles with respect to their cross-linking. For the production of a porous membrane, a bicontinuous microstructure must form so that afterward one of the two phases can be selectively extracted [8,15].

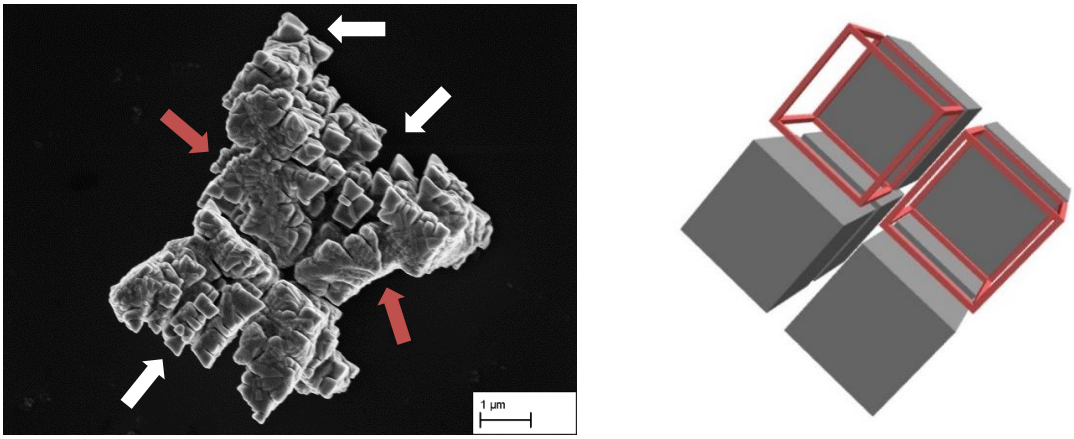

(**a**) (**b**)

Figure 5. (**a**) Extracted γ′-particle from the specimen cooled to 950 °C. Fine, coherent cubes in the outer regions (white arrows). Semi-coherent interfaces in the center (splitting channel of the original cube; red arrows). (**b**) Schematic representation of the particle, red-framed parts are no longer present on the left, giving a clear view of the central γ-channel.

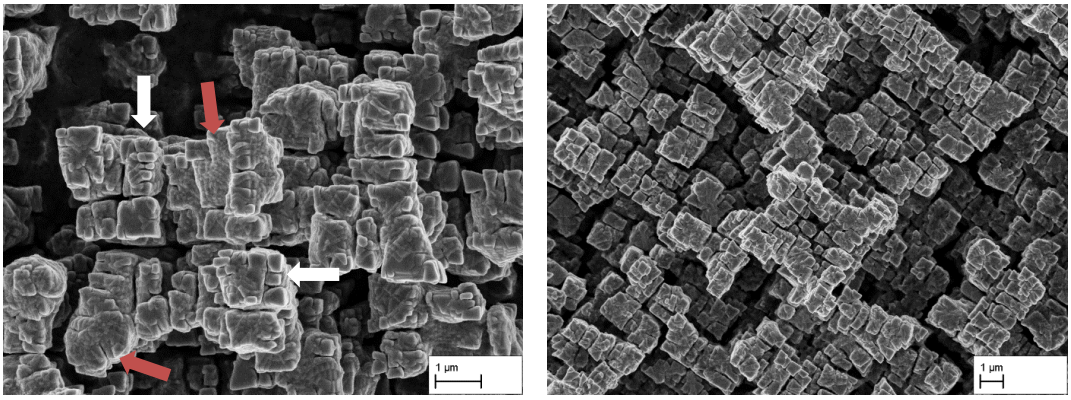

(**a**) (**b**)

Figure 6. Large and closely adjacent γ′-precipitates in deeply etched specimens; (**a**) 975 °C—neighboring particles that have grown together at their arms. Both, large areas with steps at the interfaces (see red arrows) and fine coherent parts (see white arrows) can be seen; (**b**) 900 °C—blocky, less in <111>-direction elongated, precipitates with clearly visible matrix channels between the individual particles.

Despite the very close proximity of particles at temperatures starting from about 1000 °C, 975 °C at the latest, without large precipitation-free regions between them, only a few cross-links are observed. Some particles are connected, but these often appear to have evolved from nuclei that originated relatively close to each other, so that the arms grew into each other early on (Figure 6a). If two nuclei develop at some distance, they tend to border each other in a face-to-face fashion and remain separated by a narrow matrix channel.

Looking at the surface of the deeply etched specimen with low magnification, one can get an impression of the cross-linking. If cross-linking is complete and a bicontinuous microstructure is established, the etched surface will remain at its original position. This is not the case for any temperature as shown exemplarily for the samples cooled to 1025 °C, 975 °C and 900 °C, respectively (see Figure 7). In these images, a recess of the deeply etched area situated on the side of the dotted line marked with "NC" (not coated) relative to the area which was protected by a lacquer (C; coated), is clearly visible. Therefore, one must conclude that a bicontinuous γ/γ′-microstructure does not form during slow cooling at 1 K/min alone. An additional extended isothermal heat treatment as performed in [15] is apparently required.

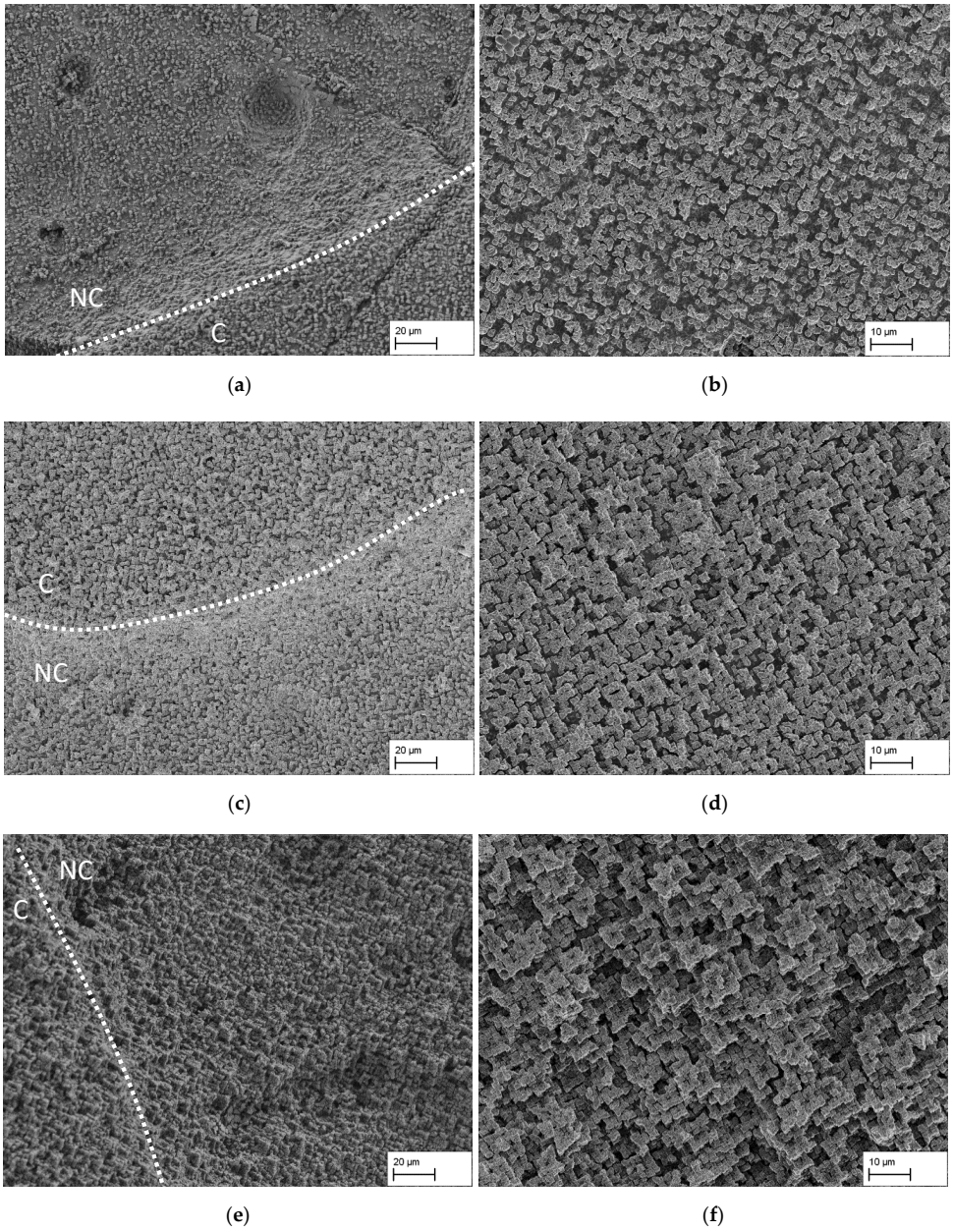

Figure 7. Surfaces of the deeply etched specimen. In each case, the transition between coated (C) and not coated area (NC) is marked by a dotted line. Here a recess of the deeply etched area is visible, which shows that a complete connection of the γ′-particles to a continuous network is not established. On the right-hand side, an image of the not coated area is shown at higher magnifications, showing γ′-particles either protruding further from the surface if they are connected or as long as they remain as individual ones causing less rough surfaces; (**a**) 1025 °C—uniform roughness; (**b**) 1025 °C—individual precipitates which are connected to the deep lying matrix that has not yet been extracted; (**c**,**d**) 975 °C—visible further protruding precipitates, due to cross-linking. (**e**) Surface roughness at the transition area in the specimen cooled to 900 °C; (**f**) 900 °C—several layers of precipitates cross-linked with each other and protruding far from the "extraction plane" (i.e., up to which the matrix was removed).

Further information can be gained from the roughness of the deeply etched surfaces. Only those precipitates are still present at the surface that are either connected to the deep lying matrix that has not yet been extracted or to other precipitates. Connected particles protrude further from the surface than individual ones, causing rougher surfaces. This effect also can be seen in Figure 7. Down to about 1000 °C, the etched surfaces remain fairly

smooth. However, below that temperature, the roughness tends to increase with decreasing temperature. This demonstrates that cross-links between γ′-particles begin to form below about 1000 °C.

4. Discussion

Based on the microstructures of the first three samples, removed from the furnace at 1185 °C, 1175 °C and 1165 °C, it is evident that the primary precipitation of γ′-particles is only to be found after cooling to 1165 °C due to the slow cooling from the single-phase state. The γ′ solvus temperature of 1185 °C according to calculations in Thermo-Calc, as mentioned in the method section, is therefore either overestimated or the cooling inside the specimen is delayed to such an extent that nucleation does not yet occur up to a set oven temperature of 1175 °C. (The temperature mentioned corresponds in each case to the temperature at the temperature sensor or the thermocouple on the sample surface.)

At both temperatures of 1185 °C and 1175 °C, a bidisperse microstructure can be seen, but the nucleation density and precipitation morphology do not match the slow cooling at 1 K/min. It is more likely that nucleation has not yet occurred during slow cooling and that the precipitation of the cubic particles is due to the opening of the furnace door and the time it takes for removing the specimen from inside the furnace and to dip them into the water bath. As a recording of the temperature using thermocouples has shown, the temperature at the sample surface drops abruptly by up to 30 K with the opening of the furnace door, and in the few seconds it takes to remove the specimen and drop it into the water bath, the temperature drops even further. The supercooling and short period of time are apparently sufficient for a high nucleation and rapid growth of the particles. The increase in the size of the cubic precipitates from about 50 nm (1185 °C), to 80 nm (1175 °C) to about 120 nm (1165 °C) can be attributed to the lower initial temperature and thus greater undercooling of the respective samples. The still visible very fine precipitates are relatively constant in size in all three samples with a diameter of about 20 nm. These particles are therefore attributed to the cooling of the specimen in the water bath, where it is known that a high nucleation density with a small particle size is to be expected.

The rapid growth of the nuclei is not surprising, since the concentration of solute elements near the nucleation sites is initially very high. With further growth, the diffusion paths increase. This can also be seen in the γ′-particles formed during cooling to 1165 °C. Within a short time, these particles have grown strongly and have undergone various morphological changes from sphere to cube to octocube and octodendrite in less than 10 min. Depending on small differences in the time of the nucleation, particles of different sizes and morphological stages are formed. In all cases, the splitting of the particles into octocubes has already occurred. In [21], it is demonstrated that splitting has its source in elastic anisotropy. Hence, above a critical size, the sum of the elastic and interfacial energy of an octocube falls below that of a single cube and splitting takes place. Comparable results have been obtained by finite element simulations [22,23].

There are different opinions on whether the splitting starts in the center of the particles [24–26] or at their outer interfaces [18,27–29]. The first theory suggests that splitting occurs by reverse precipitation of a matrix-phase particle in the center of the precipitate. Due to the concentration gradient within the square particle, the center of the particle comes closer and closer to the compositional equilibrium of the matrix phase as it grows. After a nucleus for the matrix phase has formed, anisotropic growth occurs along elastically soft directions. The second theory states that the morphological instability of the concave interfaces during cooling causes the splitting; references [28,29] show that the elastic strain is concentrated around the concave cube surfaces (simulation in 2D, here transferred to the 3D case), which generates a dissolving driving force at the surface and the groove penetrates into the interior of the particle.

Based on the present results on the morphology of the central octocubes, splitting from the surface of the precipitates inwards seems much more plausible. For example, in Figure 2e one of the three {100}-channels is continuous, namely (100). The (010)-channel is

discontinuous in at least one place—where the [1$\overline{1}\overline{1}$]-arm is still connected (on the lower right). Furthermore, on the left half in the center, directly at the (100)-channel, is a bright spot that looks like a small fracture area (see arrow in Figure 2e). At this spot, another arm seems to have been connected, which has broken off as a result of the extraction. Finally, on the (001)-channel, the formation of the channel from the outside can be clearly seen. The findings in Figure 2e do not preclude the possibility that the first (continuous) channel originates from the center of the particle and further splitting occurs from the surface. Simulations suggesting this sequence of events can be found in [26]. From Figure 3a, however, it is clear that the very center of the primary particle does not show any splitting. The fracture area interrupts all three channels (one of them is interrupted beyond this spot), which clearly eliminates the possibility that the splitting occurs exclusively from the inside to the outside.

The fine particles around the primary γ'-precipitates indicate the diffusion zones of the solute elements. These zones influence the growth of the particles since solute elements have to diffuse towards the precipitates. Based on their extent, the potential influence of neighboring precipitates can be estimated. A lower diffusion rate due to nearby particles would lead to a reduction in the growth rate. However, as can be seen in Figure 1, the diffusion zones hardly influence each other. Due to the low nucleation rate and the resulting large distance between the precipitates, the particles can initially grow without being influenced by their neighbors. This results in the star shape of the precipitates, a non-equilibrium shape, which can also be seen in the small cubic precipitates with concave surfaces.

The star-like morphology does not result from a favorable stress distribution formed by it. On the contrary, purely from a morphological point of view, the star shape has energetic disadvantages compared to cubes or octocubes, since the star-shaped morphology leads to a relatively large surface area and the dendrite surfaces do not lie on {100}-planes and thus do not form low elastic stresses. The stress distributions of different γ'-morphologies were studied in [23] using finite element simulation. Concave interfaces develop due to kinetic effects caused by supersaturation and chemical driving force. The cube corners are more exposed to the diffusion flux of oncoming solute elements, resulting in preferential growth in <111>-directions. As soon as the supersaturation of the matrix vanishes, this kinetic effect also disappears and the morphology changes again. A quasi-equilibrium shape then develops, with surfaces aligned along {100}-planes [20]. This diffusion-induced growth towards areas not yet depleted can also be seen in Figure 1. Based on the diffusion zones, it is clear that the tips of the dendrite arms are much closer to areas that are still supersaturated, so that faster growth at these points is easy to understand.

During further cooling, the present precipitates continue to grow and new ones are formed. Due to the higher amount of precipitates and the direct neighborhood to other particles, the growth is now significantly slowed down compared to the beginning. Furthermore, more nucleation sites are created due to further supercooling. After the rapid growth to large particles with many cube-like outgrowths as in Figure 4, the diffusion of solute elements is no longer unhindered and the neighboring precipitates limit the growth. The diffusion zones overlap now very strongly, so that the kinetic influences on the morphology and thus the elongation of the arms in <111>-directions decrease. However, with further cooling, the volume fraction of the precipitation phase continues to increase. Due to spatial hindrance by other precipitates, only growth of the concave surfaces is now possible. This can also be seen in Figure 3b. The right particle, as can be discerned from its size, was formed much later and is located in the area of influence of the left precipitate. This hinders the growth and stretching of the arms in the <111>-direction, especially seen in the shorter primary arm facing the left precipitate. Furthermore, this causes the morphology to change earlier from kinetically influenced to stable based on coherency stresses. This is expressed in a stronger formation of the secondary branches with surfaces parallel to {100} and thus a growth into the spaces between the dendrite arms, see also [18].

In general, the coherency of the particles is continuously decreasing with ongoing cooling. For example, after cooling to 1150 °C, Figure 4a, step-like interfaces can be seen in the center of the particle, indicating a large number of interfacial dislocations. The perfectly coherent interfaces in the splitting channel seen in Figure 2a have become much more irregular in the course of growth. As a result, the orientation of the interfaces along {100} is no longer energetically preferred and less smooth surfaces are created.

These incoherent surfaces (the interfaces actually never become truly incoherent, there are actually always interfacial dislocations, i.e., partially coherent interfaces) are visible after cooling to 950 °C on the "inner surfaces" in Figure 5a as well. This tendency of coherency loss can be seen especially on the splitting channel of the original cube (see red arrows). Overall, down to low temperatures, "half" particles can be found, i.e., particles where one half of the octodendrite is still embedded in the residual matrix while the other part was not connected during extraction and is therefore no longer present. This presence of half particles shows that the precipitates are still divided. As the temperature decreases, the frequency of visible splitting channels decreases until at 900 °C they are found very rarely.

In the exterior regions, however, the branches of the precipitates continue to be more or less coherent and cube-like. They have quite small dimensions and continue to form surfaces parallel to {100} because of the energetically more favorable distribution of coherency stresses. Between these branches are again very fine γ-channels, which may simply separate individual cubic outgrowths or may be a result of the splitting of these outgrowths. The important point to note is that coherency is not only decreasing with ongoing cooling but also from the outside to the inside of a particle.

According to the theory of [21], for coherent, cubic precipitates and low volume fractions, the particles repel when they are close and attract when they are widely separated. Repulsion prevents coalescence into larger particles, while attraction causes particles that are well separated to arrange themselves into groups. Now at temperatures below 1000 °C, these particles are no longer coherent everywhere, and the particle volume fraction is large. However, the morphology suggests that coherency stresses and elastic interactions continue to have a large influence on the particles; these extreme surfaces cannot be explained otherwise. In the exterior regions of the "giant particles", cubic and coherent outgrowths are still found (Figure 5a). Furthermore, Figure 6 shows that even in this state the precipitates do not attempt to coalesce, indicating that repulsive forces are still present when the particles come close to each other. Therefore, it is likely that the qualitative findings in [21] are valid in this case as well so that coalescence is hindered by repulsive forces as long as the particles remain coherent at their exterior.

Furthermore, in the case of γ′-precipitates with $L1_2$ ordered structure, coalescence of particles that have nucleated independently leads to antiphase domain boundaries (APB) in three out of four cases [30]. However, for coherent particles, the energy of an APB is greater than twice the interfacial energy that would be reduced during coalescence. Thus, coalescence of neighboring particles is unlikely from this point of view as long as the exterior remains coherent.

Now looking again at the former splitting channels, it is at first surprising that despite the already early loss of coherency (already after cooling to 1150 °C, Figure 4a, these inner surfaces are no longer sufficiently coherent) these subvolumes of a former single particle do not grow together again. Both repulsive forces between coherent interfaces and the formation of ABPs cannot matter here. However, observations show that only at 900 °C hardly any "half" particles can be found. In order for a single particle to coalesce again in the center, this matrix channel would have to transform completely into γ′ again. Now, however, a very narrow and long γ-channel is present there, which geometrically hinders the diffusional flow of solute elements from the outside into the channel. Furthermore, the solute elements inside the channel are alone insufficient for the particle to grow back together. For example, considering the difference in equilibrium states between 1150 °C and 950 °C, about another 35% of γ′ is likely to precipitate. Therefore, it is clear that, firstly,

a maximum of one third of the channel can transform in this example and, secondly, that the reconnection of split particles can only occur partially and at quite low temperatures.

This means that there are two different reasons why cross-linking of the particles is prevented—the repulsion of the particles due to the coherent outer regions and the initial splitting along with late reconnection of the individual subvolumes. The rare appearance of "half" particles at 900 °C shows that the particles along the former splitting channels mostly grew together again. Thus, one requirement for the particles to be able to cross-link completely with each other is essentially fulfilled. Nevertheless, as visible in Figure 7e,f, even after cooling to 900 °C, only very weak cross-linking occurs. Although some particles have grown together, as can be seen from the protruding γ′-clusters, this amount is very small in relation to the entire sample. If the particles were sufficiently cross-linked with each other, instead of this uneven, rough surface, a uniform plane would have to be created, the surface of which would be the same as the previously polished surface. Thus, it is to be concluded that the second condition, namely the connection of particles along their outer surfaces, is incompletely met even after cooling to 900 °C. According to this, the cross-linking to a bicontinuous γ/γ′-microstructure, as found in [15], only develops during isothermal aging (where slow cooling for membrane fabrication only continues to 1100 °C).

For the fabrication of superalloy membranes in [15], further aging for 144 h is performed after which the precipitates become everywhere, i.e., even at the outside, incoherent and the microstructure bicontinuous. Thus, we observe for 115NC that during slow cooling first incoherent interfaces develop. However, coherency still exists on the particle exterior, thus, preventing coalescence. Further aging for an extended period of time is required to transform the particle exterior to incoherent interphases as well so that the elastic repulsion vanishes. Due to the loss of coherency, the interfacial energy between γ′ and the matrix becomes larger than half of the APB energy so that even this barrier can now be overcome. This is supported by observations of [27], where a nickel alloy with coherent, aligned precipitates was isothermally aged. After 72 h this aging results in the precipitates becoming rounded and coalescing with their neighbors. The coalescence was much more pronounced after 336 h. The reason for these morphological changes is the coherency loss between the precipitates and the matrix, causing the coherency strains to disappear.

The overall idea of how the precipitating particles grow as they slowly cool from above the γ′ solvus temperature is as follows. Initially, individual nuclei are formed with little or no overlap between their influence zones. The particles grow to a certain size and split into subvolumes to reduce the sum of the elastic and interfacial energy, with channel formation rather from the outside to the inside than the other way around. Due to kinetic effects, i.e., better solute supply at the corners of the particles, their arms grow in the <111>-directions. Through increasing influence of the coherency stresses, steps are formed on the edges of these arms with their faces aligned parallel to {100}. This condition is shown in Figure 2. With further growth, the diffusion fields of the precipitates start to overlap and due to coherency stresses, further morphology changes occur, forming large precipitates with extreme surfaces, now covered with cube-like outgrowths (Figure 4). As the particles grow closer to each other, they can no longer increase in diameter. The increasing γ′ volume fraction now forms on the former cube faces and causes the precipitate to grow in such a way that the elongation in <111> is reduced. The result is an arrangement of large, blocky γ′-precipitates, which are adjacent to their neighbors but do not touch them. Due to elastic repulsion between the coherent parts of the precipitates and the formation of APBs, if the particles were to coalesce, these particles keep separated. With further cooling, the interfaces of the precipitates become increasingly incoherent (Figure 6a). Particles that were separated due to splitting start to coalesce again on the surfaces of former splitting channels and also begin to interconnect with neighboring particles. Due to this decreasing coherency, the elastic repulsion between particles also decreases and the loss in γ/γ′-interface energy due to coalescence overcompensates the energy required to generate APBs. Since APBs cannot play a role in the coalescence of the former octocubes (the eight cubes do not nucleate independently), the coalescence at the splitting channels is

significantly more pronounced at an earlier stage. Also, the center of the precipitates always showed more incoherent interfaces than the outer areas, which favors this reconnection despite the problem of fewer solute elements in the channel. In Figure 6b, the octodendrites have now grown back together into dendrites (at least partially reconnected) and formed some cross-links to neighboring precipitates. However, complete cross-linking and thus the formation of a bicontinuous γ/γ'-microstructure does not occur even after cooling to 900 °C. Only through further loss of coherency by isothermal aging does this happen.

Prior to this study, we assumed that coalescence of individual γ'-particles happens directly as the dendrite arms grow in <111>-directions and touch each other. However, as the outermost interfaces of the growing particles remain coherent for most of the cooling process to 900 °C, this coalescence is apparently prevented by repulsive forces due to elastic interactions and due to the likelihood of APB-formation if the particles were to coalesce. For these reasons, the γ'-particles stay separated from each other for a remarkable long time during cooling, even though they come very close to each other. Only after much longer cooling than to the temperature of 1100 °C used for the fabrication of incoherently coarsened membranes [15], namely 900 °C, very few particles have coalesced on their exterior. At this stage, dendritic growth is already no longer observed. The stretching in the <111>-directions occurs due to kinetic effects, which decrease more and more as soon as the γ'-precipitates massively grow near each other. At 900 °C, large blocks can then already be observed, and the growth of the <111>-arms is no longer prevalent.

5. Conclusions

In this paper, the growth of γ'-precipitates in the nickel-based superalloy 115NC during slow cooling at 1 K/min from supersolvus to 900 °C was studied. A major focus was on the coalescence of the particles with respect to the formation of a bicontinuous microstructure for the fabrication of metallic membranes.

During growth, the γ'-precipitates undergo several morphological changes. After a very rapid splitting into octocubes, the particles grow and form star shapes. On the surfaces of the particles, several cube-like coherent outgrowths form successively. Due to spatial hindrance of neighboring particles, they cannot increase in diameter and further γ' grows on the former cube faces of the precipitates, reducing the elongation in <111>-directions. The star shape is now changing into a blocky morphology.

Although the distance between two particles is very small, they do not grow together for the following reasons: first, elastic repulsion exists between the small, coherent cube-like outgrowths in the outer areas of the precipitates. Second, the likelihood of APB formation hinders coalescence. In addition to neighboring particles not coalescing, the narrow splitting channels of the individual precipitates do not completely transform back into γ' during further cooling, and thus only form partial connections again late in the cooling process. The overall weak cross-linking can be shown by the surface roughness, as seen in the SEM at low magnification.

Furthermore, based on the three-dimensional microstructure it was shown that splitting of γ'-precipitates with γ-nucleation in the center is very unlikely. The channels are, therefore, formed by a morphological instability at the particle surface and grow inwards.

The results show that the interfaces of the precipitates have to become incoherent in order for the particles to cross-link, which is essential for membrane production. Therefore, subsequent heat treatment for an extended period of time is indispensable for membrane fabrication. Only then the loss of coherency at the outermost interfaces is sufficient for the γ'-particles to build a continuous network.

Author Contributions: Conceptualization, J.R. and C.V.; methodology, C.V.; validation, C.V.; investigation, C.V.; resources, J.R.; writing—original draft preparation, C.V.; writing—review and editing, J.R.; visualization, C.V.; supervision, J.R.; project administration, J.R.; funding acquisition, J.R. All authors have read and agreed to the published version of the manuscript.

Funding: This research was funded by Deutsche Forschungsgemeinschaft (DFG, German Research Foundation), grant number RO 2045/36-1. We also acknowledge support by the Open Access Publication Funds of Technische Universität Braunschweig.

Data Availability Statement: Not applicable.

Conflicts of Interest: The authors declare no conflict of interest.

References

1. Pineau, A. Influence of uniaxial stress on the morphology of coherent precipitates during coarsening—Elastic energy considerations. *Acta Metall.* **1976**, *24*, 559–564. [CrossRef]
2. Pollock, T.M.; Argon, A.S. Directional coarsening in nickel-base single crystals with high volume fractions of coherent precipitates. *Acta Metall. Mater.* **1994**, *42*, 1859–1874. [CrossRef]
3. Louchet, F.; Hazotte, A. A model for low stress cross-diffusional creep and directional coarsening of superalloys. *Scr. Mater.* **1997**, *37*, 589–597. [CrossRef]
4. Matan, N.; Cox, D.C.; Rae, C.; Reed, R.C. On the kinetics of rafting in CMSX-4 superalloy single crystals. *Acta Mater.* **1999**, *47*, 2031–2045. [CrossRef]
5. Rösler, J.; Mukherji, D. Design of Nanoporous Superalloy Membranes for Functional Applications. *Adv. Eng. Mater.* **2003**, *5*, 916–918. [CrossRef]
6. Rösler, J.; Näth, O.; Jäger, S.; Schmitz, F.; Mukherji, D. Fabrication of nanoporous Ni-based superalloy membranes. *Acta Mater.* **2005**, *53*, 1397–1406. [CrossRef]
7. Rösler, J.; Näth, O. Mechanical behaviour of nanoporous superalloy membranes. *Acta Mater.* **2010**, *58*, 1815–1828. [CrossRef]
8. Rösler, J.; Voelter, C. Nanoporous Superalloy Membranes: A Review. *Adv. Eng. Mater.* **2018**, *20*, 1701011. [CrossRef]
9. Epishin, A.; Link, T.; Bruckner, U.; Fedelich, B.; Portella, P. Effects of Segregation in Nickel-Base Superalloys: Dendritic Stresses. In *Superalloys, Proceedings of the Tenth International Symposium on Superalloys, Champion, PA, USA, 19–23 September 2004*; International Symposium on Superalloys; TMS: Warrendale, PA, USA, 2004; pp. 537–543. ISBN 087339576X.
10. Hinze, B.; Rösler, J.; Schmitz, F. Production of nanoporous superalloy membranes by load-free coarsening of γ′-precipitates. *Acta Mater.* **2011**, *59*, 3049–3060. [CrossRef]
11. Krause, W. CMSX-4 Gefügeoptimierung für die Membranherstellung. Master's Thesis, Technische Universität Braunschweig, Braunschweig, Germany, 2013.
12. Rösler, J.; Krause, W.; Hinze, B. A Concept for the Control of Pore Size in Superalloy Membranes. *Metals* **2014**, *4*, 1–7. [CrossRef]
13. Tychsen, J. *Untersuchung zum Einfluss der Ausscheidungswärmebehandlung auf die Struktur nanoporöser Superlegierungsmembranen aus Nimonic 115 NC. Studienarbeit (Student Research Project)*; Technische Universität Braunschweig: Braunschweig, Germany, 2016.
14. Sasse, D. *Untersuchung zum Einfluss des Umformgrades und der Vergröberungsschritte auf die Struktur nanoporöser Superlegierungsmembranen aus Nimonic 115 NC. Studienarbeit (Student Research Project)*; Technische Universität Braunschweig: Braunschweig, Germany, 2016.
15. Voelter, C.; Rösler, J. Polycrystalline Superalloy Membranes Produced by Load-Free Coarsening of Incoherent γ′-Precipitates: Microstructure Evolution and Mechanical Properties. *Materials* **2021**, *14*, 784. [CrossRef]
16. Schmitz, F.; Rösler, J. Nanoporous Membranes Produced from Polycrystalline Ni-Based Superalloys. *J. Nanosci. Nanotechnol.* **2010**, *10*, 6256–6259. [CrossRef]
17. Koul, A.K.; Gessinger, G.H. On the mechanism of serrated grain boundary formation in Ni-based superalloys. *Acta Metall.* **1983**, *31*, 1061–1069. [CrossRef]
18. Grosdidier, T.; Hazotte, A.; Simon, A. Precipitation and dissolution processes in γ/γ′ single crystal nickel-based superalloys. *Mater. Sci. Eng. A* **1998**, *256*, 183–196. [CrossRef]
19. Ricks, R.A.; Porter, A.J.; Ecob, R.C. The growth of γ′ precipitates in nickel-base superalloys. *Acta Metall.* **1983**, *31*, 43–53. [CrossRef]
20. Wang, Y.; Khachaturyan, A.G. Shape instability during precipitate growth in coherent solids. *Acta Metall. Mater.* **1995**, *43*, 1837–1857. [CrossRef]
21. Khachaturyan, A.G.; Semenovskaya, S.V.; Morris, J.W. Theoretical analysis of strain-induced shape changes in cubic precipitates during coarsening. *Acta Metall.* **1988**, *36*, 1563–1572. [CrossRef]
22. Glatzel, U.; Feller-Kniepmeier, M. Calculations of internal stresses in the γ/γ′ microstructure of a nickel-base superalloy with high volume fraction of γ′-phase. *Scr. Metall.* **1989**, *23*, 1839–1844. [CrossRef]
23. Müller, L.; Glatzel, U.; Feller-Kniepmeier, M. Modelling thermal misfit stresses in nickel-base superalloys containing high volume fraction of γ′ phase. *Acta Metall. Mater.* **1992**, *40*, 1321–1327. [CrossRef]
24. Wang, Y.; Chen, L.-Q.; Khachaturyan, A.G. Kinetics of strain-induced morphological transformation in cubic alloys with a miscibility gap. *Acta Metall. Mater.* **1993**, *41*, 279–296. [CrossRef]
25. Liu, L.; Chen, Z.; Wang, Y. Elastic strain energy induced split during precipitation in alloys. *J. Alloys Compd.* **2016**, *661*, 349–356. [CrossRef]
26. Liu, L.; Chen, Z.; Wang, Y.; Zhang, M. The split of dendritic precipitates with interfacial anisotropy in solid transformations in alloys. *J. Alloys Compd.* **2017**, *703*, 321–329. [CrossRef]
27. Yoo, Y.S.; Yoon, D.Y.; Henry, M.F. The effect of elastic misfit strain on the morphological evolution of γ′-precipitates in a model Ni-base superalloy. *Metals Mater.* **1995**, *1*, 47–61. [CrossRef]

28. Kim, J.Y.; Yoon, J.K.; Kim, Y.C.; Suck, H.K.; Kim, K.B.; Cha, P.R. Phase Field Study for Self-Assemble of the Second Phase Particles in Coherent Phase Transition. In *Advances in Nanomaterials and Processing, Proceedings of the IUMRS-ICA-2006, International Conference in Asia, Jeju, Korea, 10–14 September 2006*; Advances in Nanomaterials and Processing; Ahn, B.T., Ed.; Trans Tech Publications Ltd.: Stafa-Zürich, Switzerland, 2007; pp. 583–586. ISBN 978-3-908451-31-0.
29. Cha, P.; Yeon, D.; Chung, S. Phase-field study for the splitting mechanism of coherent misfitting precipitates in anisotropic elastic media. *Scr. Mater.* **2005**, *52*, 1241–1245. [CrossRef]
30. Wang, Y.; Banerjee, D.; Su, C.C.; Khachaturyan, A.G. Field kinetic model and computer simulation of precipitation of L12 ordered intermetallics from f.c.c. solid solution. *Acta Mater.* **1998**, *46*, 2983–3001. [CrossRef]